AIAA JOURNAL
Vol. 57, No. 9, September 2019

Application of Resonant Femtosecond Tagging Velocimetry in the 0.3-Meter Transonic Cryogenic Tunnel

Daniel Reese* and Paul Danehy†
NASA Langley Research Center, Hampton, Virginia 23681
Naibo Jiang,‡ Josef Felver,§ and Daniel Richardson§
Spectral Energies, LLC, Dayton, Ohio 45430
and
James Gord¶
U.S. Air Force Research Laboratory, Wright–Patterson Air Force Base, Ohio 45433

DOI: 10.2514/1.J057981

Selective two-photon absorptive resonance femtosecond laser electronic excitation tagging (STARFLEET) velocimetry is demonstrated for the first time in a NASA Langley Research Center wind tunnel with high-repetition-rate and single-shot imaging. Experiments performed in the 0.3 m transonic cryogenic tunnel allowed for testing at 300 K in gaseous nitrogen over a range of pressures (124–517 kPa) and Mach numbers (0.2–0.8) for freestream conditions and flow behind a cylindrical model. Measurement precision and accuracy are determined for the current set of experiments, as are signal intensity and lifetime. Precisions of 3–5 m/s (based on one standard deviation) were typical in the experiment; precisions better than 2% of the mean velocity were obtained for some of the highest-velocity conditions. Agreement within a mean error of 3 m/s between STARFLEET freestream velocity measurements and facility data acquisition system readings is demonstrated. STARFLEET is also shown to return spatially resolved velocity profiles, although some binning of the signal is required to achieve the reported measurement precision.

Nomenclature

A	=	area, m^2
C_p	=	specific heat, constant pressure, $J/(kg \cdot K)$
g	=	gravitational acceleration, m/s^2
I	=	intensity, arbitrary units (a.u.)
P	=	pressure, Pa or kPa
T	=	temperature, K
t	=	time, s
u	=	velocity, m/s
Δ	=	generic change
ρ	=	density, kg/m^3
σ	=	standard deviation or precision
τ	=	time constant, μs

Subscripts

DAS	=	data acquisition system
i	=	spatial index (x, y, z)
j	=	frame index
rms	=	root mean square
t	=	total or stagnation
0	=	initial

Presented as Paper 2018-2989 at the 2018 Aerodynamic Measurement Technology and Ground Testing Conference, Atlanta, GA, 25–29 June 2018; received 4 October 2018; revision received 6 May 2019; accepted for publication 14 June 2019; published online 15 July 2019.

*Research Engineer, Advanced Measurements and Data Systems, National Institute of Aerospace. Member AIAA.
†Senior Technologist, Advanced Measurements and Data Systems. Associate Fellow AIAA.
‡Research Scientist. Associate Fellow AIAA.
§Research Scientist. Member AIAA.
¶Principal Research Chemist, Aerospace Systems Directorate. Fellow AIAA.

I. Introduction

GROUND-TESTING at flight-accurate Reynolds numbers is imperative for the continued safety and success of flight vehicle research and development. Transonic cryogenic tunnels (TCTs) such as the National Transonic Facility at the NASA Langley Research Center allow testing in this regime because they have been shown to reach Reynolds numbers exceeding 4×10^8 m^{-1} [1]. This is achieved by injecting cold nitrogen into the flow, which reduces the viscosity and increases the density of the flow by creating a high-pressure low-temperature environment. Although operating under these conditions produces flight-accurate Reynolds numbers, it demands sturdy construction of the facility (and any hardware needed for measurements) in order to withstand the high pressures and thermal stresses present during testing. This often leads to extremely limited optical access to the test section, making many measurement techniques difficult (or impossible) to carry out in TCTs. In addition to these physical limitations, organizational and facility regulations can often impede the use of certain measurement techniques. In some TCTs, techniques such as particle image velocimetry and Doppler global velocimetry are disallowed due to their dependence on tracer particles being introduced into the flow because these tracer particles can damage sensitive facility components or condense on test models, causing surface roughness. As such, diagnostics are traditionally limited to integrated force and moment measurements, or other onbody measurements through the use of pressure- and temperature-sensitive paint. Offbody measurements in TCTs remain limited mainly to probes, although a few laser-based techniques have been used in TCTs, as recently reviewed by Burns et al. [2–6].

One class of diagnostics that has proven effective in producing offbody velocity measurements in TCTs is molecular tagging velocimetry (MTV). MTV techniques such as femtosecond laser electronic excitation tagging (FLEET) and picosecond laser electronic excitation tagging (PLEET) do not require the addition of tracer particles and have been successfully employed in the NASA Langley Research Center's 0.3 m TCT [7,8]. FLEET and PLEET velocimetries work by focusing an ultrafast laser pulse to directly excite and dissociate molecular nitrogen (N_2); upon recombination of

the nitrogen atoms, light is emitted and can be tracked over two or more frames to provide an estimate of the local flow velocity, and potentially acceleration. In addition to their application in the 0.3 m TCT, these methods have been used to study the limitations on high-spatial-resolution measurements of turbulence [9], make velocity measurements in air and nitrogen jets [10], make hypersonic freestream and turbulent boundary-layer measurements in Arnold Engineering Development Center's Tunnel 9 [11], make three-component velocity and acceleration measurements [12], and make simultaneous temperature and velocity measurements in air [13], as well as velocity measurements in argon/argon–nitrogen gas mixtures [14] and R134a/R134a–air mixtures [15]. Femtosecond laser tagging has also been conducted using the second and third harmonics, and it has shown that the third harmonic allows for lower energy density and narrower tagged lines as compared with the second harmonic or traditional FLEET [14]. Although FLEET and PLEET lend themselves to use in TCTs due to their ability to provide unseeded velocity measurements in N_2, both techniques have physical limitations that must be considered. Perhaps the most important factor to consider with these MTV techniques is the large thermal perturbation resulting from the excitation process [16–18]. Furthermore, the high laser powers used can potentially damage wind-tunnel windows and models. These drawbacks of FLEET and PLEET can be mitigated using selective two-photon absorptive resonance FLEET (STARFLEET) [17].

STARFLEET is an additional member of the MTV class of velocimetry techniques, and it uses a 202.25 nm femtosecond laser to resonantly excite nitrogen [17]. The technique has been previously demonstrated in a laboratory-scale jet flow using low-speed cameras and multishot accumulations [17]. By frequency quadrupling an 809 nm laser (a similar wavelength as typically used for nonresonant FLEET), the overall amount of energy required to excite the nitrogen is reduced by about a factor of 30 [17], thus drastically decreasing the thermal perturbation introduced by the measurement technique. Unfortunately, the advantage of reduced energy input from the laser system is not without its downsides. The deep UV wavelengths required for optimized excitation make transmitting the laser beam over long distances difficult, and they necessitate the use of special windows and optics. Consequently, in this study, magnesium fluoride (MgF_2) windows and lenses were required to allow passage of the laser light into the wind-tunnel test section and to write the STARFLEET line.

The experimental campaign described within this paper constitutes the first application of STARFLEET velocimetry in a wind tunnel, as well as the first application of high-speed single-shot STARFLEET. Although not necessarily required for this application, STARFLEET was employed in order to explore what measurements may be possible with this technique, as well as determining the precision and accuracy that may be achievable in a large-scale facility such as the 0.3-m TCT so that these values are known in cases where minimal perturbations are required (such as thermometry). Data were obtained and analyzed for freestream conditions at 300 K covering nine flow conditions, including pressures from 124 to 517 kPa (18 to 75 psi) and Mach numbers from 0.2 to 0.8. This paper continues with a description of the experimental setup in Sec. II, whereas Sec. III discusses the data processing. Results such as freestream velocity measurements, as well as precision and accuracy estimates, are presented in Sec. IV; and final conclusions are drawn in Sec. V.

II. Experimental Setup

Experiments were conducted in the NASA Langley Research Center's 0.3 m TCT: a closed-loop fan-driven cryogenic wind tunnel. Although the tunnel is capable of running with several different test gases, only nitrogen was used in the present studies for the ability to obtain the highest Reynolds numbers and for optimal performance of STARFLEET. The facility has a 0.33×0.33 m test section surrounded by a pressurized plenum, and it is capable of stably operating at total pressures ranging from 124 to 517 kPa, with total temperatures from 100 to 325 K and Mach numbers from 0.2 to 0.85. An array of wall

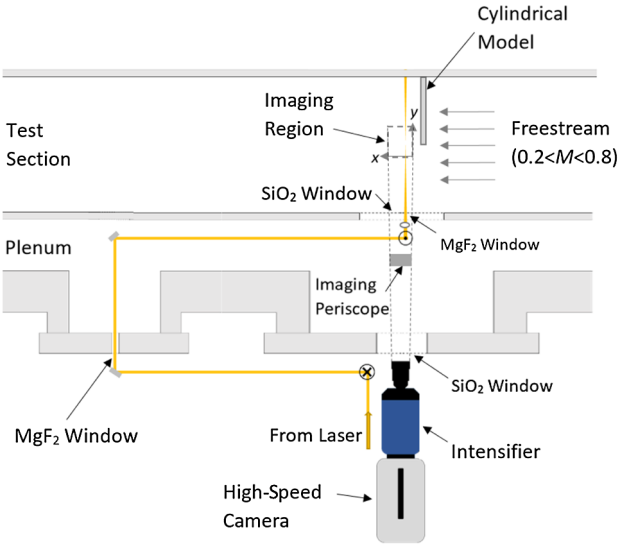

Fig. 1 Schematic of the experimental setup as seen from above.

pressure taps, thermocouples, pitot probes, pressure transducers, and strain gauges make up the facility data acquisition system (DAS), and DAS instrument readings were used as a basis of comparison for results obtained from STARFLEET measurements. Fused silica (SiO_2) windows in the test section and outer plenum provided optical access for the camera, whereas magnesium fluoride (MgF_2) windows allowed for laser penetration into the test section. A schematic showing the experimental setup (including a layout of the camera, laser path, optics, plenum, and test section) is shown in Fig. 1.

A regeneratively amplified Ti:sapphire laser system (Spectra-Physics Solstice) with a repetition rate of 1 kHz, a temporal bandwidth of 92 fs, a center wavelength of 809 nm, and a bandwidth of 13 nm was used as input to a frequency quadrupler [19] in order to create the 202.25 nm light that was used to write the STARFLEET line. Although the laser system produced approximately 60 μJ per pulse at the exit of the quadrupler, only 8 μJ per pulse were present inside of the test section. This large drop in power was caused by the combined effect of absorption of the UV laser propagating through air, as well as additional losses incurred at each mirror (typically with 85% reflectivity) and window (~92% transmission). Before passing through the test section MgF_2 window, the laser beam was focused using a 250 mm MgF_2 spherical lens in order to write the STARFLEET line. Due to the lower laser energy and the slower optics used to focus the beam, these studies used less than 1/20th of the laser power to write the STARFLEET line as compared with that used in the STARFLEET work of Jiang et al. [17]. It should be noted that these substantial power differences could potentially have a significant effect on the STARFLEET signal and N_2 recombination mechanism, and further investigation into these differences may be warranted.

STARFLEET signal was recorded using a UV high-speed image intensifier (LaVision high speed intensified relay optics with an S20 photocathode) lens coupled to a high-speed complementary metal–oxide–semiconductor camera (Photron SA-Z). Imaging was done through a 100 mm focal length, $f/2$ UV Halle lens, yielding a magnification of eight. With a standoff distance of approximately 0.9 m, the collection solid angle is ~0.0024 sr, resulting in the collection of about 0.02% of the total STARFLEET signal. In future experiments, signals could be increased by using faster (lower $f/$no.) collection optics and shortening the standoff distance; however, this was not possible in the current experiment due to cost and facility constraints. For each run condition, six frames of data (with 1 μs exposure every 2.5 μs, corresponding to a rate of 400 kHz) are captured for more than 2000 sets of data. The first frame of each set is a "cleaning frame" to remove unwanted accumulated charge from the detector, the second frame is a background image used in data processing, and the last four frames contain the STARFLEET signal. Although each set contains four frames of STARFLEET data, there is only one laser pulse per set. A total of nine conditions were

investigated by changing the flow pressure ($P = 124$, 276, and 517 kPa) and Mach number ($M = 0.2$, 0.5, and 0.8). Velocity measurements were made in the freestream at varying conditions, as well as for the case of flow behind a 1-in.-diameter cylindrical model. The processing of raw data obtained in these studies is discussed further in the following section.

III. Data Analysis

Discussed in detail within this section are the various processing steps needed to obtain STARFLEET signal and velocimetry results. Section III.A outlines the preprocessing stage, which includes the dewarping, scaling, and binning of data. Section III.B covers the methods used to determine the peak signal location to subpixel accuracy from the preprocessed STARFLEET image sets. Finally, Section III.C contains an analysis of the displacement calculations to obtain spatially resolved velocity measurements.

A. Preprocessing (Signal Dewarping, Scaling, and Binning)

There are more than 2000 sets of data (2000 individual single-shot velocity measurements) for each of the nine conditions covered in these experiments, and every set contains four frames of the STARFLEET signal plus background images. The first step in the preprocessing stage is to apply an image dewarping to correct every frame for lens effects and perspective distortion resulting from the oblique camera viewing angle. This is achieved by taking a set of calibration images of a target placed such that the target face is parallel to the path of the laser in the imaging plane. This is the same method used in many similar MTV experiments, although different than prior FLEET and PLEET experiments in the 0.3 m TCT where the target was placed normal to the laser beam [2,16]. The target used in the present work consisted of a regular grid pattern of small dots, with 6.2 mm spacing between points. Dot locations in the calibration images are determined using a custom centroid-finding algorithm, and each point is then mapped to the expected location, given the known target pattern. The calculated transformation is then applied to all frames of STARFLEET data. Because the physical spacing between target dot centroids is known, this method of data dewarping also allows for the extraction of a scale factor used to calibrate the STARFLEET signal data from pixel spacing into physical units. The top row of Fig. 2a shows the raw STARFLEET signal for each of the four frames for freestream flow, and the bottom row shows the corresponding data binned to five rows for each frame. The top row of Fig. 2b shows the raw STARFLEET signal for each of the four frames of flow behind the 1-in.-diameter cylindrical model, and the bottom row shows the corresponding data binned to five rows for each frame. Sample dewarped STARFLEET images (in physical units) can be seen for freestream data along the top row of Fig. 2a, where the leftmost image is the first frame of data, and each succeeding image is the following frame within the set. In this figure, the STARFLEET line is shown as a dark, vertical line that first appears just to the left of $x = 3.2$ mm but shifts rightward as it tracks the flow with each subsequent frame. Similar results are shown for the case of flow behind a 1-in.-diameter cylindrical model along the top row of Fig. 2b, where the STARFLEET line profile clearly indicates a velocity deficit occurring near the top of the image (in the region behind the model) when compared with the bottom (in freestream flow). The image origin is approximately 50 mm behind the model, as shown in Fig. 1.

Earlier work using similar MTV techniques in the 0.3 m TCT have almost exclusively used boresight (or near-boresight) configurations wherein the camera's view of the signal is along or nearly along the laser's path [19,20]. These studies have traditionally relied on imaging signal from an integrated region along the excited line to obtain the signal-to-noise ratio (SNR) necessary to make accurate and precise single-point two-component velocity measurements. In the present work, however, an imaging geometry is used where the laser is directed into the flow through one window and the camera images through another window (parallel to the first) at an angle of approximately 40 deg to the laser, allowing for spatially resolved velocity measurements in the y direction. Several factors led to the use of this geometry in addition to the desire for spatial resolution.

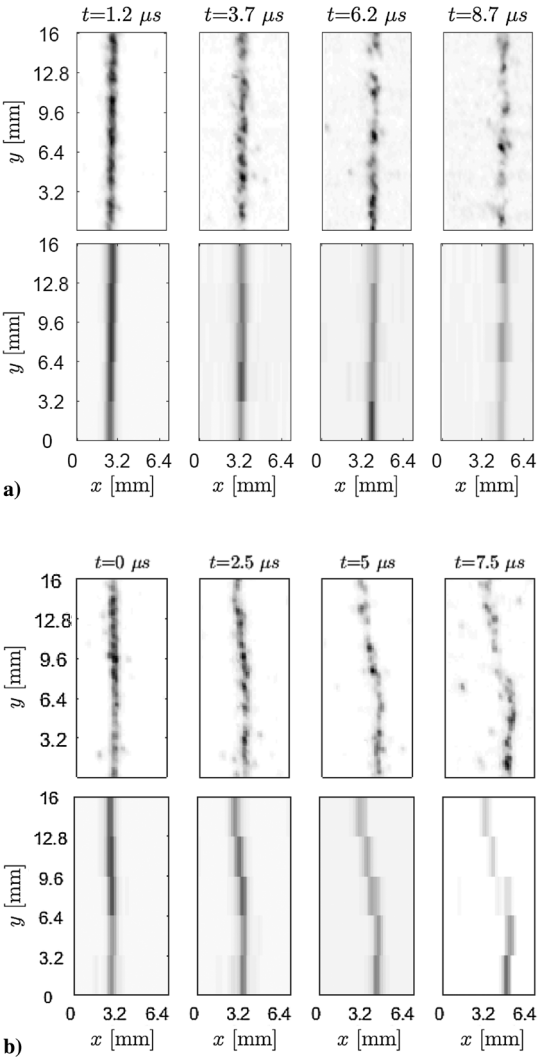

Fig. 2 Raw vs binned STARFLEET signals for a) freestream conditions and b) flow behind a cylindrical model.

First, the STARFLEET signal appears to be much longer (on the order of 20–30 mm) as compared to previous FLEET or PLEET measurements in the same facility, which used the same focusing lens, due to the smaller beam diameter used in the STARFLEET studies. Using a boresight-type configuration with STARFLEET would therefore result in an order of magnitude larger spatial averaging. Also, MgF_2 windows had to be used for the laser beams, and these windows are relatively expensive; so, small windows were used that were too small for the camera to image the signal. Consequently, the use of this geometry results in a decreased SNR as compared to the prior FLEET and PLEET experiments in this facility. The SNR in the boresight configuration is higher than the non-boresight configuration because, in the boresight configuration all of the emission is spatially integrated on a small spot on the detector. In the current experiment, this light is spread out into a line over multiple pixels. By taking the signal to be the average intensity along a small central region (approximately 16 by 1 mm) spanning the STARFLEET line, and defining the noise as the standard deviation of the residual to a Gaussian fit within the same region, a value of SNR = 3.7 was obtained for the first frame containing the STARFLEET signal. Because molecular tagging velocimetry methods work best at SNR = 4 and above [20,21], the compromised SNR from the spatially distributed signal (in addition to the already low pumping energy used to write the STARFLEET line) requires the use of binning to obtain results comparable to those found in previous studies. The effect of bin size on the precision of velocity measurements was investigated, and it served as the principal metric used to determine the bin size for further

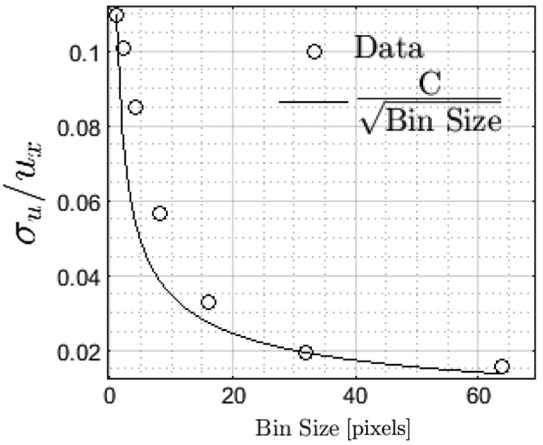

Fig. 3 Precision measurements (as percentage of mean velocity) as function of bin size. Final bin size of 20 pixels was chosen for data analysis, allowing for more precise, spatially resolved velocity estimates.

analysis. Figure 3 shows the effect of varying the bin size on the standard deviation of velocity measurements for the freestream $M = 0.8$, $P = 517$ kPa case. The first data point in Fig. 3 (bin size $= 1$) was obtained by calculating the standard deviation of velocity from dewarped and scaled STARLEET images for all sets of data for the chosen condition, and then dividing by the mean velocity. Subsequent data points were obtain by first binning the dewarped and scaled STARLEET images by the selected bin size before calculating the precision. This method of calculating precision measurements will include any actual freestream velocity fluctuations in the facility, but it does so consistently across all chosen bin sizes.

It is important to note that, although increasing bin size reduces the standard deviation of velocity, this improvement in precision comes at the cost of reduced spatial resolution. To the first order, the bin size reflects averaging over that number of samples, which results in a reduction in fluctuations by $\sqrt{\text{bin size}}$; this $C/\sqrt{\text{bin size}}$ trend is shown in Fig. 3 as a solid line. A bin size of 20 pixels was ultimately chosen because this yielded spatial resolution (∼3 mm) and precisions (2–3%) approaching previous studies [18,22] while allowing for the extraction of the velocity from five y locations spanning the wind-tunnel test section. The binned data have SNR $= 15$, and it is this binned STARFLEET signal that is used in the analysis that follows. Representative binned STARFLEET signal images are shown for freestream data along the bottom row of Fig. 2a, as well as for the case of flow behind a cylindrical model along the bottom row of Fig. 2b.

B. Determination of Peak Signal Location

The next step of the analysis entails determining the x location of the peak signal intensity for all y locations and frames within each set. The following Gaussian model is fit to the preprocessed STARFLEET data in order to determine the peak signal location with subpixel accuracy:

$$G(x) = c_0 + a_1 \exp\left[-\left(\frac{x - b_1}{c_1}\right)^2\right] \tag{1}$$

where the first term is fit to the background signal, ensuring that the second term of $G(x)$ provides a proper fit to the STARFLEET signal. From this fit, an x location corresponding to the peak signal intensity is extracted to subpixel accuracy for each y location and frame. The binned single-shot signal intensity for each of the four frames of data is shown in Fig. 4a as dots, and corresponding fits are shown as lines, with peak intensities/locations marked with an x. Peak signal locations are plotted as a function of time in Fig. 4b, where the slope of the fit line gives an estimate of velocity. Figure 4a shows results from all four frames of data for a single y location of the STARFLEET signal. The intensities (normalized by the maximum intensity of the set) for all four frames are shown as black points, and solid lines indicate the corresponding fit of each frame. At the peak of each fit, a black x indicates the measured location of the peak STARFLEET signal. Once the peak signal location has been determined for all y locations and frames within a set, this position information can be used to determine velocity using a number of different velocity estimation schemes. Details on the method chosen for use in the present work are provided in the following subsection.

C. Velocity Calculations

Because more than two frames of the STARFLEET signal were obtained in the current study, there are several ways to extract velocity estimates once peak signal locations have been determined. Burns and Danehy [22] and Burns et al. [23] conducted a study of various schemes (including point to point, linear regression, and polynomial fitting) and showed that the linear regression method exhibited the highest measure of accuracy and precision. In this work, a similar linear fit to the peak signal location in time is performed to calculate flow velocity, with several constraints introduced (detailed in the following) to ensure that only valid and physical velocity results are considered.

The first restriction applied to the data was that only locations determined from intensities above a certain threshold were included in the velocity fit; because the background signal is nominally constant at around five counts throughout this set of experiments, this condition ensures that frames with a low SNR are rejected. This restriction eliminated about 3.5% of the frames. Next, the fit was required to pass through the first peak signal location, even if a better R^2 value could have been attained by allowing the fit to intercept the position axis at a location different than that of the initial point. Finally, all velocity fits with $R^2 < 0.97$ were excluded from consideration. This restriction eliminated a further 2% of the data. A typical linear fit to peak signal location in time is shown in Fig. 4b. Each peak signal location determined by the method described in Sec. III.B (and shown as a black x in Fig. 4a) is shown as a black x in Fig. 4b, whereas the fit to these data is shown as a solid line. The velocity for this set of data is determined by the slope of the fit line. This analysis method is appropriate for the measurement of freestream flows where acceleration and steep gradients are expected to be negligible.

IV. Results and Discussion

This section highlights the STARFLEET results obtained from experiments in the 0.3 m TCT. Section IV.A covers the signal intensity and lifetime measurements of the STARFLEET signal over a range of tunnel operating conditions. Velocity measurements,

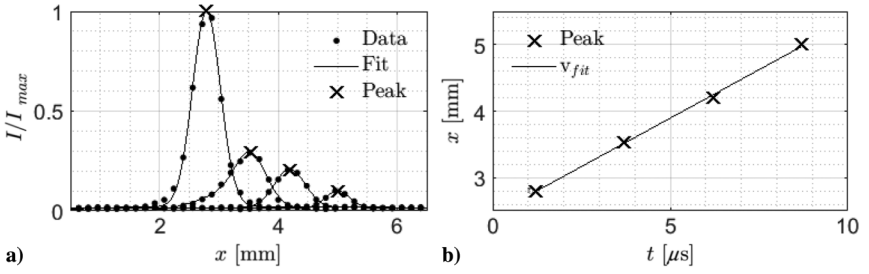

Fig. 4 Determination of peak signal location and velocity calculation. a) Binned single-shot signal intensity (normalized by the maximum intensity) for each of four frames of data. b) Peak signal locations plotted as a function of time, where the slope of the fit line gives an estimate of velocity.

including profiles and comparison with facility values, are displayed and discussed in Sec. IV.B. Lastly, the precision and accuracy of the velocity results are studied in Sec. IV.C.

A. Signal Intensity and Lifetime Measurements

Using the peak signal intensity for each y location and frame determined as in Sec. III.B, the sensitivity of the STARFLEET signal to the flow pressure and Mach number can be investigated. Figure 5a shows the absolute intensity measurements as a function of time for various pressures and Mach numbers (stars indicate the signal lifetimes for each case). Figure 5b shows the normalized intensity measurements, showing that the largest intensity values give the most rapid signal decay. Figure 5c shows the intensity as a function of static pressure for all four frames of data from the $M = 0.8$ case. Figure 5d shows the lifetime measurements as a function of static pressure, indicating that higher pressures correspond to shorter lifetimes The effect of varying the pressure and Mach number on signal intensity is shown in Fig. 5a, where the circular, square, and triangular symbols differentiate flow pressures; and line types indicate various Mach numbers. The same data are shown normalized to the first frame intensity in Fig. 5b, which more clearly shows the effect of different flow conditions on signal lifetime measurements. The three solid line fits to the data of the constant Mach number ($M = 0.8$) reveal that the STARFLEET signal increases with increasing pressure. The effect of the Mach number is also demonstrated in Figs. 5a and 5b (with $M = 0.2, 0.5$, and 0.8 indicated by the dotted, dashed, and solid lines, respectively), and it shows a reduction in the measured peak intensities with increasing Mach number, for a given total pressure P_0. This observation can be explained by the reduced static pressure owing to a higher Mach number because the STARFLEET signal intensity is shown to decrease with a reduction of static pressure. This effect is shown for the high–Mach-number case in Fig. 5c where, at least for short delays, an increase in flow pressure causes an increase in signal intensity.

In addition to providing insight into the sensitivity of the signal to flow conditions, intensity measurements were also used to determine the STARFLEET signal lifetime, which has important implications for making high-precision measurements. As conducted in similar MTV experiments [23], signal intensity decay is fit as a function of time using a biexponential model:

$$I(t) = ae^{bt} + ce^{dt} \tag{2}$$

The signal lifetime can then be defined to be the time that the signal reaches $1/e$ of the value at the earliest delay time. Biexponential fits are shown as lines in Figs. 5a and 5b, whereas stars indicate the measured lifetimes for each case. The signal lifetime measurements are also shown as a function of static pressure for the high–Mach-number case in Fig. 5d. The data suggest that static pressure has a significant effect on the lifetime with increasing pressures decreasing the lifetimes, which is in agreement with the FLEET technique [23]. Residual scatter in the data may be attributed to the different static temperatures at different Mach numbers, although the static temperature varied less than 15% over the range of conditions in this plot.

B. Velocity Measurements

Velocity profiles were calculated for each set and all conditions for both the freestream data and flow behind a 1-in.-diameter cylindrical model. Figure 6a shows the mean velocity profiles for the $M = 0.8$, $P = 517$ kPa case, with the measured velocity at each y position as a percentage of the freestream velocity; whereas Fig. 6b shows the corresponding rms profiles. Figure 6a shows the mean velocity profiles for both the freestream case and for flow behind a cylinder,

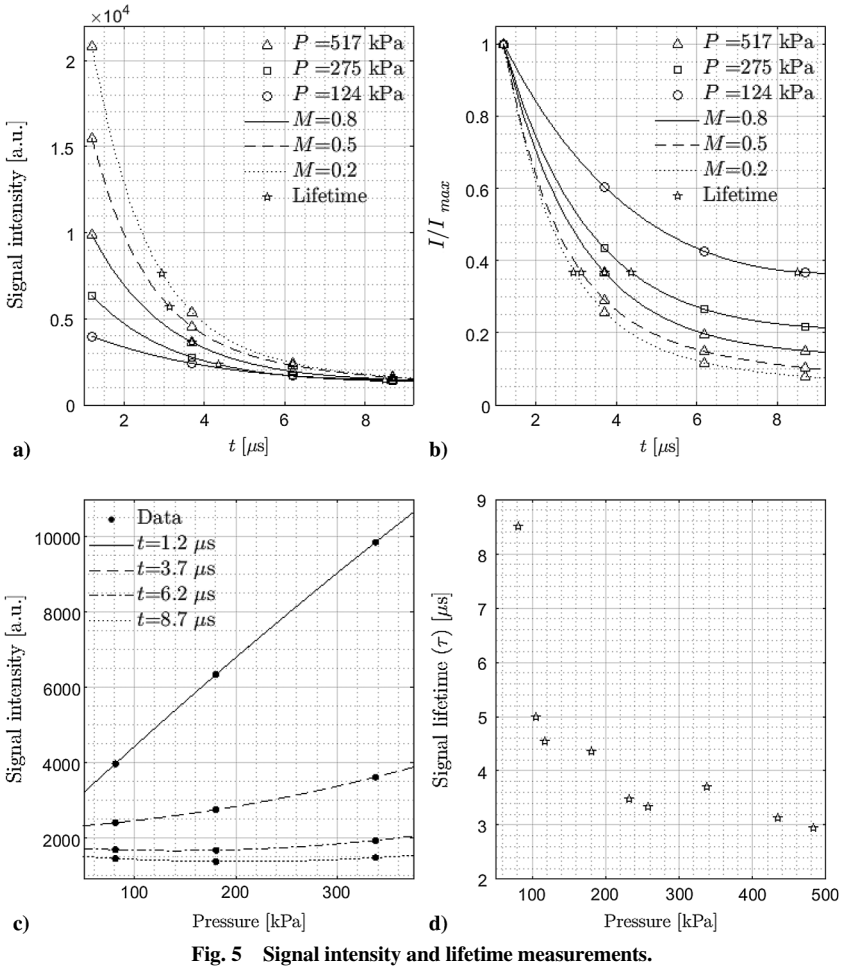

Fig. 5 Signal intensity and lifetime measurements.

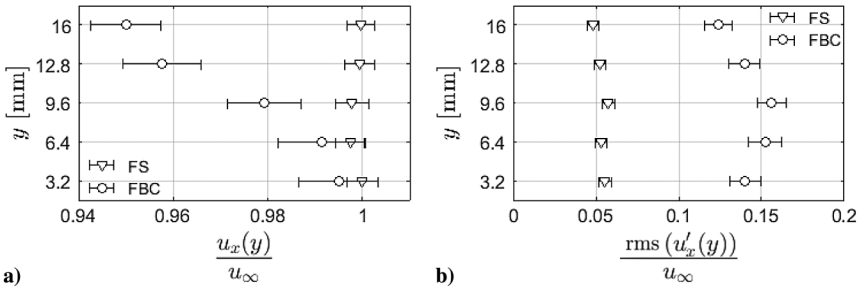

Fig. 6. Representations of a) mean velocity and b) rms profiles for the freestream (FS; triangles) and flow behind a cylindrical model (FBC; circles). Error bars indicate uncertainty in the mean.

and the error bars indicate the uncertainty in the mean ($U_m = 2\sigma/\sqrt{N_{\text{sets}}}$) at each y location. As demonstrated in Fig. 6a, the freestream profile shows nearly constant velocity across the tunnel test section, whereas the profile corresponding to the case of flow behind a cylinder indicates a velocity deficit in the region behind the model. The profiles in Fig. 6b show that rms values for flow behind a cylindrical model are nearly three times that of the freestream case, with the largest values occurring in the center of the rms profile.

In addition to spatially resolved measurements, freestream velocity profiles (such as the one shown in Fig. 6) were collapsed to a single value for each set by averaging the velocities from each of the five y locations; all 2000+ sets were then averaged to yield a single mean velocity measurement for each run condition and an uncertainty in that mean. Velocity measurements for all nine cases considered in this study are summarized in Fig. 7, where they are compared against facility DAS measurements. No uncertainty error bars are seen because they are smaller than the sizes of the symbols used. A more detailed analysis of the precision and accuracy of the STARFLEET velocity measurements is carried out in the following section.

C. Measurement Precision and Accuracy

As with previous unseeded velocimetry techniques applied in high-pressure cryogenic wind tunnels [7,8], accuracy measurements are made by comparison to the facility DAS values of velocity, and results are summarized in Fig. 7 for all nine conditions covered in the present work. Although the measured STARFLEET velocities generally tend to agree well with those reported by the facility DAS, the discrepancy appears to grow larger with increasing velocity. The maximum error between STARFLEET and DAS measured mean velocities was 7.7 m/s (corresponding to 2.9% of the freestream velocity), whereas the mean error was 3 m/s. This discrepancy could be partly caused by an error in calibration because the target used for calibration could have been slightly out of alignment with the path of the laser and/or the dewarping algorithm might not have sufficiently removed perspective distortion in the STARFLEET images. Additionally, with single-line tagging methods, such as that used in the present work, there is an inherent error in the estimated velocity normal to the tagged line due to the unknown velocity component parallel to the line [24]. A multi-time-delay method was proposed as a solution to these errors associated with single-line tagging [25], although this method was not applied in the current work because these errors are negligible for the case of uniform, freestream flow perpendicular to the tagged line (which is the case for a majority of the results considered in this paper).

One standard deviation of the velocity measurements is taken to be the precision, which is shown as a fraction of the measured velocity in Fig. 8. Precision as a percentage of the mean velocity is shown to generally decrease with increasing Mach number, as well as to decrease with increasing pressure. The dashed line in this figure represents the trend of the optimal precision across all Mach numbers based on a measured "wind off" velocity of 3 m/s. Precisions better than 2% of the mean velocity were obtained for some conditions. Although nearly all precision measurements lie below 4% of the freestream velocity, the worst-case precision measurement is near 7%, owing, in part, to a low mean velocity in the denominator and low initial signal occurring at low pressure. These single-shot precision measurements correspond to a roughly constant value of 3–5 m/s, with the percent precision decreasing for higher freestream velocities due to the larger denominator. In general, these precision

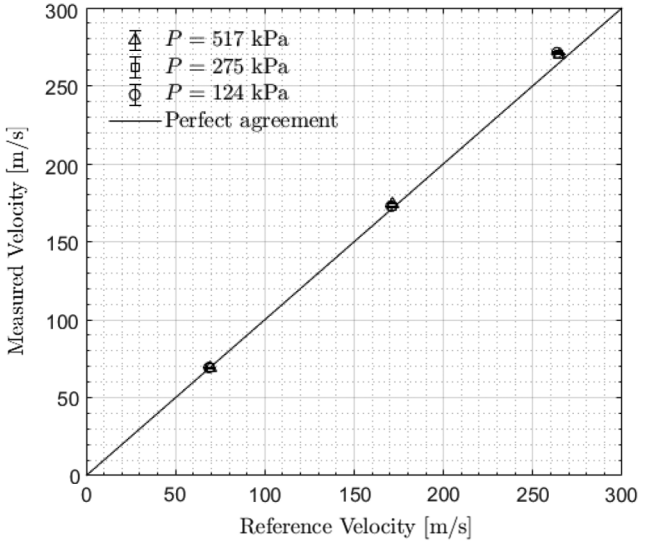

Fig. 7 STARFLEET velocity measurements compared with facility DAS readings. Error bars are present but hidden by data points. The solid line indicates perfect agreement.

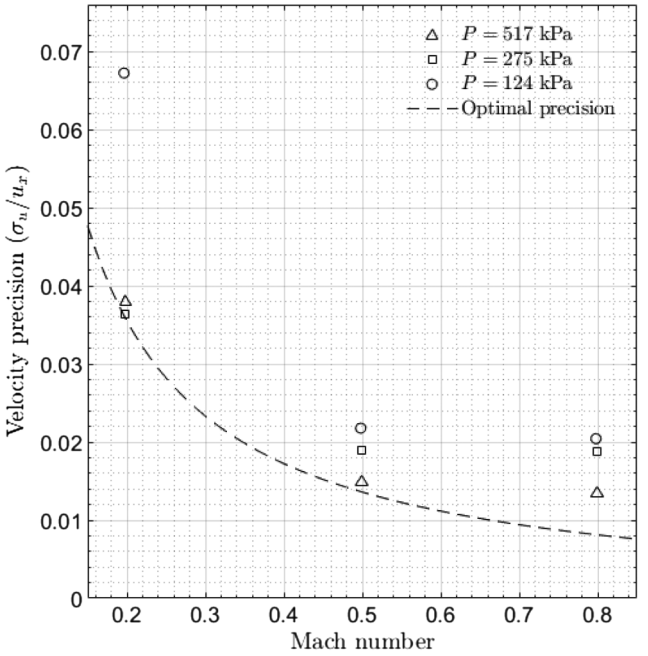

Fig. 8 Precision (as a fraction of the mean freestream velocity) as a function of stagnation pressure and Mach number.

measurements are an order of magnitude larger than results from similar MTV measurements made in the 0.3 m TCT using FLEET [22].

V. Conclusions

For the first time, high-repetition-rate and single-shot STARFLEET velocimetry has been successfully demonstrated in a wind tunnel. The main advantage of STARFLEET is the lower energy required in the test section to make the measurement, which reduces the perturbation to the flow. The NASA Langley Research Center's 0.3 m transonic cryogenic tunnel allowed for flow measurements at 300 K over a wide range of Mach numbers and pressures. Signal intensity and lifetime dependence on these conditions were explored, and a reduction in intensity was shown for both increasing Mach number and decreasing pressure. The precision and accuracy of mean freestream velocity measurements were also explored. Precision was shown to generally be 3–5 m/s, which was typically 2–4% of the freestream value; and agreement within a mean error of 3 m/s between STARFLEET velocity measurements and facility DAS readings was demonstrated. Spatially resolved velocity profiles were obtained for both the freestream and the flow behind a cylindrical model, and the STARFLEET method was shown to be sufficiently sensitive to measure the velocity deficit in the region behind the model.

Although measurements in this study showed STARFLEET to be less precise than previous similar FLEET and PLEET measurements in the 0.3 m TCT, it is important to note that several important factors lead to this result. First, a large number of mirrors were used in this study, which lead to very low energy in the wind-tunnel facility; this can be easily improved in future experiments by reducing the total number of mirrors used to deliver the laser beam to the test section. Additionally, the imaging configuration allowed for a spatially distributed signal, whereas previous experiments used the boresight configuration. As demonstrated in Fig. 3, by collapsing all data to a single bin (reducing the spatial resolution to mimic the boresight configuration of earlier work), more precise measurements similar to those in previous studies can be attained; although, even then, the precision is worse than prior FLEET and PLEET results. Although FLEET allows for precise velocity measurements without the use of a fourth-harmonic generator and PLEET allows for high-repetition-rate measurements, STARFLEET is an important addition to nonintrusive MTV measurement techniques that significantly reduces thermal perturbations in the flow of interest.

Acknowledgments

This work was supported by a NASA Langley Research Center Internal Research and Development (IRAD) Project and NASA's Aerosciences Evaluation and Test Capabilities Portfolio, as well as NASA's Small Business Innovation Research (SBIR) NNX14CL74P and NNX15CL24C, and the U.S. Air Force Office of Scientific Research award nos. 15RQCOR202 and 14RQ06COR. The authors wish to thank Sukesh Roy of Spectral Energies, LLC for his support during this project. Additional thanks goes to the staff at the 0.3 m transonic cryogenic tunnel for their support, including Wes Goodman, Mike Chambers, Cliff Obara, Tammy Price, Karl Maddox, and Reggie Brown.

References

[1] Fuller, D. E., "Guide for Users of the National Transonic Facility," NASA TM-83124, 1981.

[2] Burns, R. A., and Danehy, P. M., "Unseeded Velocity Measurements Around a Transonic Airfoil Using Femtosecond Laser Tagging," *AIAA Journal*, Vol. 55, No. 12, 2017, pp. 4142–4154. doi:10.2514/1.J056154

[3] Quest, J., and Konrath, R., "Accepting a Challenge—The Development of PIV for Application in Pressurized Cryogenic Wind Tunnels," *41st AIAA Fluid Dynamics Conference and Exhibit*, AIAA Paper 2011-3726, 2011. doi:10.2514/6.2011-3726

[4] Willert, C., Stockhausen, G., Beversdorff, M., Klinner, J., Lempereur, C., Barricau, P., Quest, J., and Jansen, U., "Application of Doppler Global Velocimetry in Cryogenic Wind Tunnels," *Experiments in Fluids*, Vol. 39, No. 2, 2005, pp. 420–430. doi:10.1007/s00348-004-0914-z

[5] Gartrell, L. R., Gooderum, P. B., Hunter, W. W., and Meyers, J. F., "Laser Velocimetry Technique Applied to the Langley 0.3-Meter Transonic Cryogenic Tunnel," NASA TM-81913, 1981.

[6] Honaker, W. C., and Lawing, P. L., "Measurements in the Flow Field of a Cylinder with a Laser Transit Anemometer and a Drag Rake in the Langley 0.3-m Transonic Cryogenic Tunnel," NASA TM-86399, 1985.

[7] Burns, R. A., Peters, C. J., and Danehy, P. M., "Unseeded Velocimetry in Nitrogen for High-Pressure, Cryogenic Wind Tunnels, Part 1: Femtosecond-Laser Tagging," *Measurement Science and Technology*, Vol. 29, No. 11, 2018, Paper 115302. doi:10.1088/1361-6501/aade1b

[8] Burns, R. A., Danehy, P. M., Jiang, N., Slipchenko, M., Felver, J., and Roy, S., "Unseeded Velocimetry in Nitrogen for High-Pressure Cryogenic Wind Tunnels, Part 2: Picosecond-Laser Tagging," *Measurement Science and Technology*, Vol. 29, No. 11, 2018, Paper 115203. doi:10.1088/1361-6501/aade15

[9] Edwards, M. R., Limbach, C., Miles, R. B., and Tropina, A., "Limitations on High-Spatial-Resolution Measurements of Turbulence Using Femtosecond Laser Tagging," *53rd AIAA Aerospace Sciences Meeting, AIAA SciTech Forum*, AIAA Paper 2015-1219, 2019. doi:10.2514/6.2015-1219

[10] Peters, C. J., Danehy, P. M., Bathel, B. F., Jiang, N., Calvert, N. D., and Miles, R. B., "Precision of FLEET Velocimetry Using High-speed CMOS Camera Systems," *31st AIAA Aerodynamic Measurement Technology and Ground Testing Conference*, AIAA Paper 2015-2565, 2015. doi:10.2514/6.2015-2565

[11] Dogariu, L. E., Dogariu, A., Miles, R. B., Smith, M. S., and Marineau, E. C., "Non-Intrusive Hypersonic Freestream and Turbulent Boundary-Layer Velocity Measurements in AEDC Tunnel 9 Using FLEET," *2018 AIAA Aerospace Sciences Meeting*, AIAA Paper 2018-1769, 2018. doi:10.2514/6.2018-1769

[12] Danehy, P. M., Bathel, B. F., Calvert, N., Dogariu, A., and Miles, R. P., "Three-Component Velocity and Acceleration Measurement Using FLEET," *30th AIAA Aerodynamic Measurement Technology and Ground Testing Conference*, AIAA Paper 2014-2228, 2014.

[13] Edwards, M., Dogariu, A., and Miles, R., "Simultaneous Temperature and Velocity Measurement in Unseeded Air Flows with FLEET," *51st AIAA Aerospace Sciences Meeting Including the New Horizons Forum and Aerospace Exposition*, AIAA Paper 2013-0043, 2013. doi:10.2514/6.2013-43

[14] Zhang, Y., and Miles, R. B., "Femtosecond Laser Tagging for Velocimetry in Argon and Nitrogen Gas Mixtures," *Optics Letters*, Vol. 43, No. 3, 2018, pp. 551–554. doi:10.1364/OL.43.000551

[15] Zhang, Y., Danehy, P. M., and Miles, R. B., "Femtosecond Laser Tagging in 1,1,1,2-Tetrafluoroethane with Trace Quantities of Air," *2018 AIAA Aerospace Sciences Meeting, AIAA SciTech Forum*, AIAA Paper 2018-1027, 2018. doi:10.2514/6.2018-1027

[16] Burns, R. A., and Danehy, P. M., "FLEET Velocimetry Measurements on a Transonic Airfoil," *55th AIAA Aerospace Sciences Meeting*, AIAA Paper 2017-0026, 2017. doi:10.2514/6.2017-0026

[17] Jiang, N., Halls, B. R., Stauffer, H. U., Danehy, P. M., Gord, J. R., and Roy, S., "Selective Two-Photon Absorptive Resonance Femtosecond Laser Electronic Excitation Tagging Velocimetry," *Optics Letters*, Vol. 41, No. 10, 2016, pp. 2225–2228. doi:10.1364/OL.41.002225

[18] Limbach, C. M., and Miles, R. B., "Rayleigh Scattering Measurements of Heating and Gas Perturbations Accompanying Femtosecond Laser Tagging," *AIAA Journal*, Vol. 55, No. 1, 2016, pp. 112–120. doi:10.2514/1.J054772

[19] Kulatilaka, W. D., Gord, J. R., Katta, V. R., and Roy, S., "Photolytic-Interference-Free, Femtosecond Two-Photon Fluorescence Imaging of Atomic Hydrogen," *Optics Letters*, Vol. 37, No. 15, 2012, pp. 3051–3053. doi:10.1364/OL.37.003051

[20] Gendrich, C. P., and Koochesfahani, M. M., "A Spatial Correlation Technique for Estimating Velocity Fields Using Molecular Tagging Velocimetry (MTV)," *Experiments in Fluids*, Vol. 22, No. 1, 1996,

pp. 67–77.
doi:10.1007/BF01893307

[21] Ramsey, M. C., and Pitz, R. W., "Template Matching for Improved Accuracy in Molecular Tagging Velocimetry," *Experiments in Fluids*, Vol. 51, No. 3, 2011, pp. 811–819.
doi:10.1007/s00348-011-1098-y

[22] Burns, R. A., Danehy, P. M., Halls, B. R., and Jiang, N., "Application of FLEET Velocimetry in the NASA Langley 0.3-Meter Transonic Cryogenic Tunnel," *31st AIAA Aerodynamic Measurement Technology and Ground Testing Conference*, AIAA Paper 2015-2566, 2015.
doi:10.2514/6.2015-2566

[23] Burns, R. A., Danehy, P. M., and Peters, C. J., "Multiparameter Flowfield Measurements in High-Pressure, Cryogenic Environments Using Femtosecond Lasers," *32nd AIAA Aerodynamic Measurement Technology and Ground Testing Conference*, AIAA Paper 2016-3246, 2016.

[24] Koochesfahani, M. M., and Nocera, D. G., "Molecular Tagging Velocimetry," *Handbook of Experimental Fluid Dynamics*, edited by J. Foss, C. Tropea, and A. Yarin, Springer–Verlag, New York, 2007, Chap. 5.4.

[25] Hammer, P., Pouya, S., Naguib, A., and Koochesfahani, M., "A Multitime-Delay Approach for Correction of the Inherent Error in Single-Component Molecular Tagging Velocimetry," *Measurement Science and Technology*, Vol. 24, No. 10, 2013, Paper 105302.
doi:10.1088/0957-0233/24/10/105302

J. M. Austin
Associate Editor